**Centrum voor Wiskunde en Informatica**
Centre for Mathematics and Computer Science

H.E. de Swart

Analysis of a six-component barotropic spectral model: chaotic motion, predictability and vacillation

Department of Applied Mathematics Report AM-R8710 December

Bibliotheek
Centrum voor Wiskunde en Informatica
Amsterdam

The Centre for Mathematics and Computer Science is a research institute of the Stichting Mathematisch Centrum, which was founded on February 11, 1946, as a nonprofit institution aiming at the promotion of mathematics, computer science, and their applications. It is sponsored by the Dutch Government through the Netherlands Organization for the Advancement of Pure Research (Z.W.O.).

Copyright © Stichting Mathematisch Centrum, Amsterdam

# Analysis of a Six-Component Barotropic Spectral Model: Chaotic Motion, Predictability and Vacillation

H.E. de Swart
*Centre for Mathematics and Computer Science*
*P.O. Box 4079, 1009 AB Amsterdam, The Netherlands*

A low-order spectral model of the barotropic potential vorticity equation in a $\beta$-plane channel is considered. Its physical and mathematical properties are investigated by a numerical bifurcation analysis of the steady states and periodic solutions. The two parameters varied are the external forcing and width-length ratio of the channel with which the topographic and barotropic instability mechanisms can be controlled, respectively. Particular interest is paid to the existence of solutions describing a flow with a limited predictability and which can vacillate between different preferent regimes. It appears that, depending on the parameter values and initial conditions, the long-term behaviour of the flow can be either stationary, periodic, quasi-periodic or chaotic. An important scenario is found which leads to the generation of strange attractors. It includes the occurrence of homoclinic orbits for specific parameter values, which connect an unstable stationary point with itself. For nearby parameter values chaotic orbits exist which move in small tubes around the homoclinic orbits, in agreement with Silnikov's theory. The chaotic motion, characterized by a positive Lyapunov exponent, describes irregular flow predictable on a time scale given by the reciprocal of this exponent. However, despite its interesting properties the model cannot describe transitions between different preferent regimes. It is argued that this is due to the structure of the equations as well as to the severe truncation of the spectral expansions.

1980 *Mathematics Subject Classification*: 86 A10, 76 E20, 34 C35.
*Key words & Phrases:* low-order model, vacillation between weather regimes, bifurcation analysis, homoclinic orbits and chaos.

## 1. Introduction

It is clearly indicated by synoptic observations that the atmospheric circulation has an irregular temporal and spatial structure. This suggests that complicated models are needed in order to describe adequately the evolution of the flow. The structure of general circulation models confirms this idea. From observations as well as from the model results it appears that the planetary-scale flow vacillates between different preferent states (so-called weather regimes). Often they are classified into three categories: a high-index regime (intense westerlies, small wave amplitudes), a low-index regime (large waves, weak zonal flow) and a transitional regime. Another characteristic property is the limited predictability of the flow, i.e. forecasts only have validity on a finite time interval of at most two weeks. These features cannot be explained by a linear theory: they are essentially a consequence of nonlinear interactions between different scales of motion.

Although general circulation models are succesful in simulating the atmospheric circulation they do not provide much insight into the underlying dynamics. It is therefore significant to investigate whether it is possible to construct simple nonlinear models which reflect the features mentioned previously. This can be done by using the spectral approach. It consists of expanding state variables in a limited number of normal modes. Substitution of these series in the equations of motion yields a finite number of coupled nonlinear ordinary differential equations:

$$\dot{x} = f_\mu(x) \qquad \text{in } \mathbb{R}^N . \tag{1.1}$$

Here $x=(x_1,x_2,\cdots,x_N)$ represents the mode amplitudes, a dot denotes differentiation with respect to time and $f_\mu(x)$ is an $N$-dimensional vectorfield depending on $x$ and parameters $\mu=(\mu_1,\mu_2,\cdots,\mu_m)$. Furthermore $N$ is the truncation number and $\mathbb{R}^N$ the phase space. Eqa. (1.1) can be analysed with

Report AM-R8710
Centre for Mathematics and Computer Science
P.O. Box 4079, 1009 AB Amsterdam, The Netherlands

techniques originating from dynamical systems theory. It is of interest to know whether they reflect properties of the atmospheric circulation. More specifically, we will investigate whether system (1.1) contains a strange attractor with a multimodal probability distribution on it. Since the associated chaotic motion is characterized by sensitive dependence on the initial conditions, it models a finite predictable flow. The multimodal probability distribution means that the trajectories alternately visit different preferent regions in phase space, as required to have an index cycle.

In this paper we will study a six-component spectral model of the barotropic potential vorticity equation in a beta channel, originally derived by CHARNEY and DEVORE (1979). These authors showed that it contains a three-component subsystem which has multiple equilibria for a wide range of parameter values. The corresponding circulation patterns show characteristics of the high-index, low-index and transitional weather regimes discussed previously. However no vacillation behaviour is obtained since the equilibria of high-and low-index type are always stable. Thus, it is useful to study the effect of including more modes in the spectral expansions. The next model in the hierarchy is the six-component model already mentioned, which is also considered in MATSUDA (1983) and YODEN (1985). A spherical analogon is discussed in KÄLLÉN (1981, 1982).

Although these studies answered many questions our knowledge of the model is still incomplete. For example, the existence of vacillatory solutions has not been investigated. Therefore, in the present paper a detailed analysis of the physical and mathematical properties of the model is presented. In section 2 a short derivation of the spectral equations is given, differing somewhat from the standard method. Recently developed numerical techniques will be used to obtain the solutions. In section 3 the steady state structure and stability properties are studied as a function of two parameters: the external forcing, controlling the topographic instability mechanism and the width-length ratio of the channel which controls the barotrophic triad interactions. It is found that the number of steady states can vary from 1 up until 11. The existence of strange attractors is investigated in the sections 4 and 5 by continuing in parameter space branches of periodic orbits which bifurcate from branches of steady states. In some cases the periodic orbits become homoclinic, such that they connect unstable equilibria with themselves. For nearby parameter values strange attractors occur, in agreement with Silnikov's theory, see SPARROW (1982) and GLENDINNING and SPARROW (1984). However, although the six-component model has interesting properties it is of limited validity for the atmospheric circulation. It appears that the strange attractors only have a small domain of attraction in phase space, such that chaotic trajectories remain in a certain regime forever. Physically, this is due to the presence of only one barotropic wave triad by which the possibility of nonlinear interactions is too restrictive. It is argued in section 6 that more degrees of freedom are needed in order to obtain vacillation behaviour.

## 2. DERIVATION OF THE SPECTRAL EQUATIONS AND METHOD OF ANALYSIS

We start with a simple model of the atmospheric circulation. Consider a quasi-horizontal flow (length scale $k^{-1}$, time scale $\sigma^{-1}$) in a barotropic atmosphere with characteristic scale height $H$. The motion is assumed to be quasi-geostrophic and takes place on a midlatitudinal $\beta$-plane, centered at the latitude $\phi=\phi_0$ of the spherical earth. Its dynamics are governed by a barotropic potential vorticity equation (PEDLOSKY, 1979). In a nondimensional form it reads

$$\frac{\partial}{\partial t}\nabla^2\psi + J(\psi,\nabla^2\psi) + \gamma J(\psi,h) + \beta\frac{\partial\psi}{\partial x} + C\nabla^2(\psi-\psi^*) = 0. \tag{2.1}$$

Here $t$ is time, $\psi(x,y,t)$ the streamfunction, $h(x,y)$ the position of the lower vertical boundary with characteristic amplitude $h_0$ and $\psi^*(x,y)$ a forcing streamfunction. All variables have been scaled according to the scheme given above. Furthermore

$$\begin{aligned} &\nabla=\left(\frac{\partial}{\partial x},\frac{\partial}{\partial y}\right) \quad , \quad J(a,b)=\frac{\partial a}{\partial x}\frac{\partial b}{\partial y}-\frac{\partial a}{\partial y}\frac{\partial b}{\partial x}\ , \\ &dx=r_0\cos\phi_0 d\lambda \quad , \quad dy=r_0 d\phi\ , \end{aligned} \tag{2.2}$$

where $\lambda$ is the longitude and $r_0$ the radius of the earth. The nondimensional parameters are

$$\gamma = \frac{f_0 h_0}{\sigma H}\ ,\quad \beta = \frac{\beta_0}{\sigma k}\ ,\quad C = \frac{f_0 \delta_E}{2\sigma H}\ , \tag{2.3}$$

where $f_0 = 2\Omega \sin\phi_0$, $\beta = (2\Omega/r_0)\cos\phi_0$, $\Omega$ the angular speed of rotation of the earth and $\delta_E$ the depth of the Ekman boundary layer near the earth's surface.

Next we apply the spectral method to (2.1), for more details see DE SWART (1987). The solution $\psi$ of (2.1) on a certain domain $D$ with boundary conditions is expanded in a series of orthonormal eigenfunctions of the Laplace operator. Assuming that $\psi^*$ and $h$ can be expanded in eigenfunctions as well, we have

$$(\psi,\psi^*,h) = \sum_j (\psi_j,\psi_j^*,h_j)\phi_j. \tag{2.4}$$

Here

$$\begin{aligned} &\nabla^2\phi_j + \lambda_j^2\phi_j = 0, \\ &<\phi_l, \phi_m> = \int_D \phi_l\phi_m^{cc}dr \Big/ \int_D dr = \delta_{lm}, \\ &j = (j_1,j_2)\ ;\ j_1,j_2 \text{ integers}, \end{aligned} \tag{2.5}$$

with $\phi_j$ the eigenfunctions and $\lambda_j^2$ the eigenvalues. Furthermore $cc$ denotes a complex conjugate and $\delta_{lm}$ is the Kronecker delta function. Each eigenfunction must obey the boundary conditions.

In this paper the motion is considered in a rectangular channel of length $L = k^{-1}$ in the zonal $x$-direction and width $B$ in the meridional $y$-direction. Note that we scale with the channel-length and not with the channel-width, as is usually done. This is done because we wish to keep the length fixed and vary the width. The boundary conditions to (2.1) are taken to be (PHILLIPS, 1954):

$$\begin{aligned} &\psi(x,y,t) = \psi(x+2\pi,y,t), \\ &\frac{\partial\psi}{\partial x} = 0 \text{ and } \frac{\partial}{\partial t}\int_0^{2\pi}\frac{\partial\psi}{\partial x} = 0 \text{ at } y=0,\ y=\pi b, \end{aligned} \tag{2.6}$$

where

$$b = \frac{2B}{L}. \tag{2.7}$$

The eigenfunctions and eigenvalues satisfying (2.5) and (2.6) are

$$\{\phi_j\}_j = \begin{cases} \sqrt{2}\cos(\dfrac{j_2 y}{b}) & ,\ \lambda_j^2 = \dfrac{j_2^2}{b^2}\ , \\ \sqrt{2}e^{ij_1x}\sin(\dfrac{j_2 y}{b}) & ,\ \lambda_j^2 = j_1^2 + \dfrac{j_2^2}{b^2}\ , \end{cases} \tag{2.8}$$

$$|j_1|,j_2 = 1,2,...$$

They consist of $(0,j_2)$ zonal-flow modes and $(j_1,j_2)$ Rossby-wave modes, respectively. A low-order model is constructed by letting $(-1,1) \leqslant \underline{j} \leqslant (1,2)$. The topography and external forcing are represented by

$$h = \cos(x)\sin(\frac{y}{b})\ ,\quad \psi^* = \sqrt{2}\psi_{01}^*\cos(\frac{y}{b}). \tag{2.9}$$

Projecting eq. (2.1) on these six eigenfunctions and introducing the real valued velocity amplitudes

$$\begin{aligned} x_1 &= \psi_{01}/b \quad , \quad x_1^* = \psi_{01}^*/b, \\ x_2 &= (\psi_{11}+\psi_{-11})/(\sqrt{2}b) \quad , \quad x_3 = i(\psi_{11}-\psi_{-11})/(\sqrt{2}b) \\ x_4 &= \psi_{02}/b \quad , \\ x_5 &= (\psi_{12}+\psi_{-12})/(\sqrt{2}b), \quad , \quad x_6 = i(\psi_{12}-\psi_{-12})/(\sqrt{2}b), \end{aligned} \tag{2.10}$$

we obtain the spectral equations

$$\begin{aligned} \dot{x}_1 &= \qquad\qquad\quad \gamma_1^* x_3 \quad -C(x_1-x_1^*) \quad , \\ \dot{x}_2 &= -(\alpha_1 x_1-\beta_1)x_3 \qquad\quad -Cx_2 \qquad\quad -\delta_1 x_4 x_6, \\ \dot{x}_3 &= (\alpha_1 x_1-\beta_1)x_2 \quad -\gamma_1 x_1 \quad -Cx_3 \qquad\quad +\delta_1 x_4 x_5, \\ \dot{x}_4 &= \qquad\qquad\quad \gamma_2^* x_6 \quad -Cx_4 \qquad\quad +\epsilon(x_2 x_6 - x_3 x_5), \\ \dot{x}_5 &= -(\alpha_2 x_1-\beta_2)x_6 \qquad\quad -Cx_5 \qquad\quad -\delta_2 x_3 x_4, \\ \dot{x}_6 &= (\alpha_2 x_1-\beta_2)x_5 \quad -\gamma_2 x_4 \quad -Cx_6 \qquad\quad +\delta_2 x_2 x_4. \end{aligned} \tag{2.11}$$

Here

$$\begin{aligned} \alpha_m &= \frac{8\sqrt{2}}{\pi}\,\frac{m^2}{4m^2-1}\,\frac{b^2+(m^2-1)}{b^2+m^2} \quad , \quad \beta_m = \frac{\beta b^2}{b^2+m^2} \quad , \\ \delta_m &= \frac{64\sqrt{2}}{15\pi}\,\frac{b^2-(m^2-1)}{b^2+m^2} \quad , \quad \gamma_m^* = \frac{4m}{4m^2-1}\,\frac{\sqrt{2}b\gamma}{\pi} \quad , \\ \epsilon &= \frac{16\sqrt{2}}{5\pi} \quad , \quad \gamma_m = \frac{4m^3}{4m^2-1}\,\frac{\sqrt{2}b\gamma}{\pi(b^2+m^2)} \quad , \end{aligned} \tag{2.12}$$

are functions of the model parameters. The equations (2.11) will be studied in this paper. CHARNEY and DEVORE (1979) analysed a system almost equivalent to (2.11) except that we have taken a time scale $\sigma^{-1}$ instead of $f_0^{-1}$ and furthermore, we have scaled with the channel-length instead of the channel-width. Consequently, our state variables differ by a factor $bf_0/\sigma$ and our nondimensional time by a factor $\sigma/f_0$.

Some discussion about the mathematical properties of (2.11) can be found in appendix A. It is a dynamical system of the type (1.1) with $N=6$. For $t\to\infty$ solutions tend to a bounded set of limit points of zero volume in phase space. We are particularly interested in the possibility that the system has internally generated vacillation behaviour. It means that for fixed parameter values trajectories should alternately visit different preferent regions in phase space. This concept requires the set of limit points to consist of a globally attracting strange invariant set with a multimodal probability distribution on it.

We remark that if initial conditions are chosen such that $x_4(0)=x_5(0)=x_6(0)=0$, the evolution will be governed by the three-component subsystem in (2.11) between the dashed lines. Its properties are simple and well-known, see also the review in DE SWART (1987). It has the possibility of three different equilibria $(E_1,E_2,E_3)$ for a wide range of parameter values. The corresponding streamfunction patterns resemble large-scale preference states of the atmospheric circulation. However, no vacillation behaviour is found. Trajectories starting from arbitrary initial conditions always tend to one of the steady states of the system. The only instability mechanism present is due to topography. Compared with this three-component model, the full model (2.11) exhibits a new physical mechanism, called barotropic instability. This is a consequence the presence of a triad interaction between the (0,2), (1,1) and (1,2) mode. Application of the Fjørtoft theorem to this triad gives (FJØRTOFT, 1953)

$$\text{if } b^2<3 : \text{(0,2) mode can become unstable,} \tag{2.13}$$

if $b^2>3$ : (1,1) mode can become unstable.

In the next sections we will study the set of limit points of (2.11) for the parameter values $C=0.1, \beta=1.25$, $\gamma=1$ and $b$ and $x_1^*$ free. The flow is confined to a channel with length 5000 km and variable width measured by $b$, see (2.7), centered at the latitude $\phi_0=45°$. Furthermore the amplitude of the topography is 1 km and the dissipation time scale 10 days. These values are representative for large-scale atmospheric flow in midlatitudes. We consider $x_1^*=Uk/\sigma$ to be a free parameter, i.e. $\sigma/k \simeq 8ms^{-1}$ and we vary the intensity $U$ of the external velocity forcing in the (0,1) zonal flow component. Note that the other free parameter, $b$, in fact controls the barotropic wave triad, see (2.13).

We will use a numerical bifurcation analysis for finding the equilibria (corresponding to steady states) and periodic orbits of the model. More information about this method is given in appendix A. Routines were used from the software package AUTO (DOEDEL, 1986) in combination with numerical time integrations.

## 3. STATIONARY SOLUTIONS AND THEIR BIFURCATIONS

First the equilibria of (2.11) and their stability properties are investigated for varying $x_1^*$ and $b$. We can distinquish between single-mode equilibria, for which the $x_4, x_5$ and $x_6$ components are zero, and the other mixed-mode equilibria. The single-mode equilibria are also stationary solutions of the three-component subsystem. As discussed previously there may be either one or three of them, depending on the parameter values.

In figure 1 curves in the $(b, x_1^*)$ parameter space are shown. Here one or more real parts of the eigenvalues of the vectorfield linearized at a stationary point are zero. The solid lines, labelled $L_1, L_2$ and $L_3$, are curves of limit points (saddle-node bifurcations). The dashed lines are curves of ordinary bifurcation points and the dotted lines, labelled H1, H2 and H3, are curves of Hopf bifurcation points. Definitions of equilibria, bifurcations etc. can be found in appendix A. At the limit points and bifurcations points two different branches of equilibria come together. Consequently, the associated curves in figure 1 divide the parameter space into regions, each with its own characteristic number of equilibria. This is denoted by the symbols $a_s, a_m$, where $a_s$ gives the number of single-mode equilibria and $a_m$ the number of mixed-mode equilibria. Stability properties of at least one of the equilibria changes each time that a curve in the diagram is crossed. They are not indicated, since the diagram is already densely filled with information. In figure $1^{b,c}$ blow-ups of two regions are presented, where the behaviour is rather complicated. Thick points in the diagram are special singular points of the model, because they are associated with bifurcations of codimension larger than one. It means that more than one free parameter is needed to describe the bifurcation adequately. For example, the unfolding near the point $(x_1^*, b) \simeq$ (5.042, 0.267) is the well-known cusp catastrophe, see appendix A. The phase-flow structure near such points can be rather complicated. Of particular interest are the points labelled A, B, C and D. There we have the coaslescence of a Hopf bifurcation and a saddle-node bifurcation. As will be discussed later on at these points a direct transition occurs from regular to chaotic solutions.

The curve L1 is the bifurcation set of the three-component subsystem, where the number of single-mode equilibria changes from one to three. From figure 1 we conclude that for $b<1.279$ the six-component model has a similar qualitative structure with only single-mode equilibria. However, if $b$ becomes larger additional mixed-mode equilibria can occur, making the bifurcation diagram more complicated. In figure 2 cross-sections of the bifurcation diagram are presented. Shown are the $\hat{x}_1$-and $\hat{x}_4$-components of the equilibria as a function of $x_1^*$ for $b=1.4, b=1.5, b=1.6$ and $b=2$. Note that the high-index equilibria ($E_1$) are always stable. When $b>1.279$ mixed-mode equilibria are generated at the branch of low-index ($E_3$) equilibria. This occurs by means of pitchfork bifurcations, which cause $E_3$ to become unstable. The bifurcations are due to topographic instability of the (1,2) Rossby mode: at this point the wave is in phase with the topography. Beyond the bifurcation, perturbations of the unstable state $E_3$ have a growing standing-wave structure.

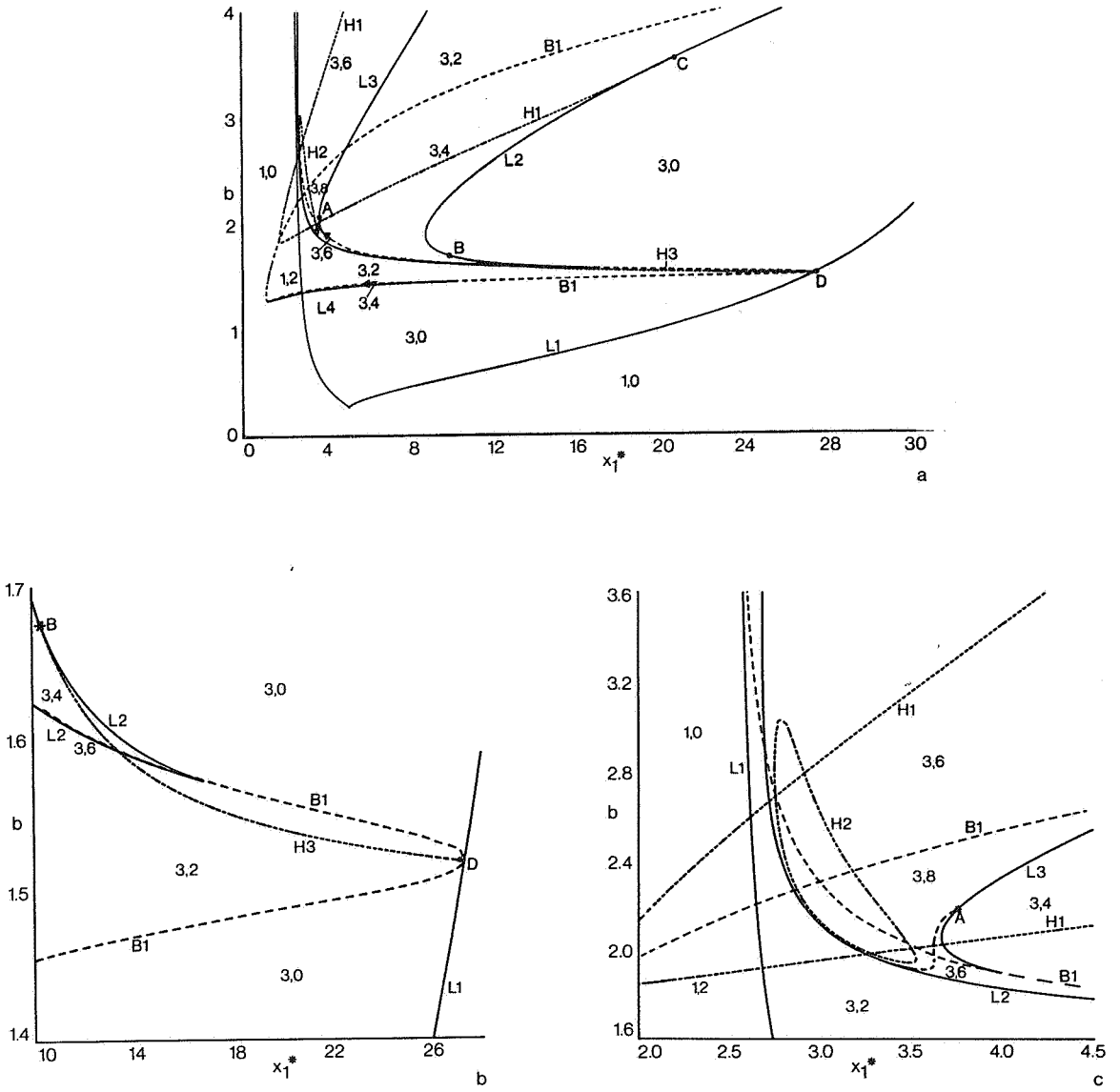


FIGURE 1 a.) Curves of singular points in the $b, x_1^*$ parameter space. Solid lines are curves of limit points (L1, L2, L3), dashed lines are curves of pitchfork bifurcations (B1) and dotted lines are curves of Hopf bifurcation points (H1, H2, H3). The symbols $a_s, a_m$ denote the number of single-mode equilibria and mixed-mode equilibria, respectively. The points $A, B, C$ and $D$ are associated with a direct transition from a regular to a chaotic behaviour.

b). Blow-up of a) : $10 < x_1^* < 28$, $1.4 < b < 1.7$.

c). Blow-up of a) : $2 < x_1^* < 4.5$, $1.6 < b < 3.5$.

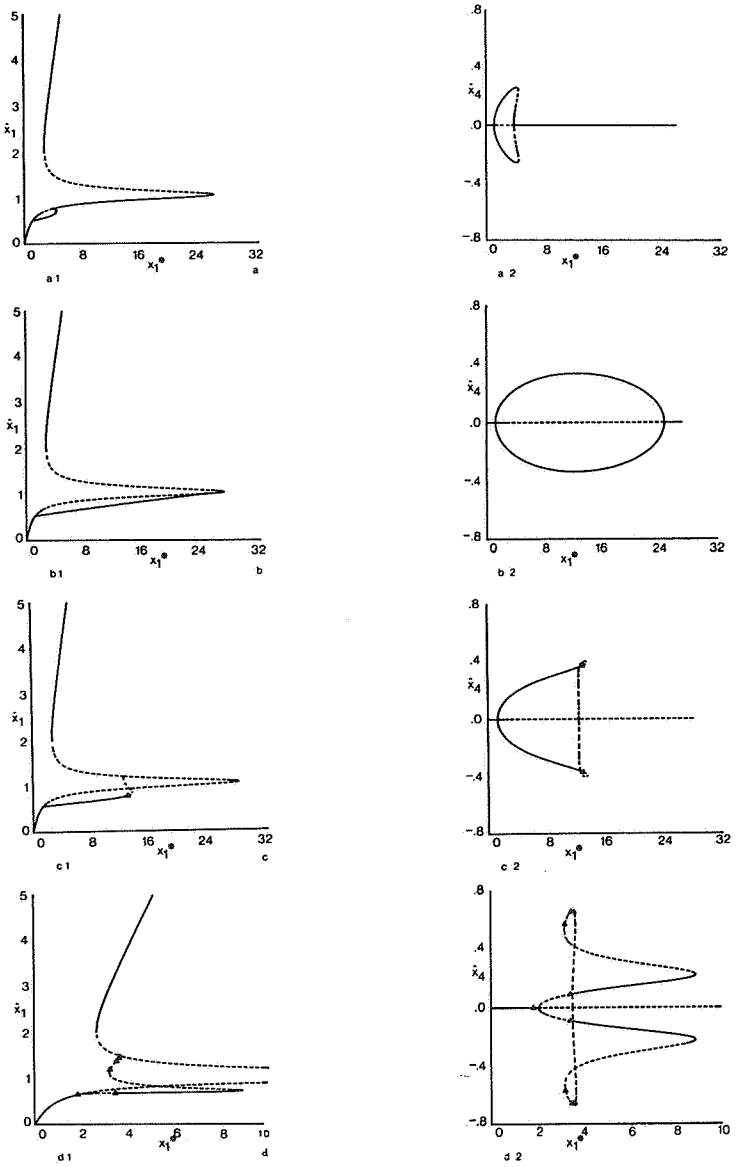

FIGURE 2. From left to right: $\hat{x}_1$-and $\hat{x}_4$-components of the equilibria as a function of $x_1^*$ for $b=1.4(a), b=1.5(b)$, $b=1.6(c)$ and $b=2.0(d)$. A solid line denotes that the solution is stable, while a dashed line indicates an unstable solution. The triangle symbol denotes a Hopf bifurcation point.

As long as $b<1.517$ mixed-mode equilibria are absorbed by the $E_3$-branch (figure $2^{a,b}$). However, if $b$ exceeds this bound they vanish at the branch of $E_2$-equilibria (figure $2^{c,d}$). Another, more important, aspect for $b>1.517$ is that equilibria can become unstable due to the presence of Hopf bifurcations, causing the generation of periodic solutions. Hopf bifurcations are a manifestation of the barotropic instability mechanism, where the periodic solutions can be interpreted as topographically modified travelling barotropic Rossby waves.

In figure 1 there is one dashed region where no stable equilibria exist. Numerical integrations show that for these parameter values trajectories starting from arbitrary initial conditions tend to a globally attracting limit cycle. Thus we conclude that the set of limit points of (2.13) at least contains a point attractor or periodic attractor.

## 4. Periodic and aperiodic solutions

### *4.1. Zonal-flow instabilities*

In figure 1 indications are present that the behaviour of the six-component model can be chaotic. To investigate the existence of strange attractors we have studied the position and stability of periodic orbits branching off from stationary points as a function of $x_1^*$. This has been done for the cases $b=1.6$ and $b=2.0$. As discussed in the previous section for these values of $b$ periodic solutions can be generated which represent barotropic travelling waves. Clearly, these values are *characteristic* for the behaviour of the model since for $b=1.6$ the (0,2) zonal-flow mode can become unstable while for $b=2$ this may occur to the (1,1) wave mode, see (2.13). Note that once the periodic orbits branch off from stationary points of the mixed-mode type, they occur in pairs. If their orbits in phase space are given as $P_\mu(\underline{x},t)=0$ and $\tilde{P}_\mu(\underline{x},t)=0$, they are related by

$$P_\mu(x_1,x_2,x_3,x_4,x_5,x_6;t) = \tilde{P}_\mu(x_1,x_2,x_3,-x_4,-x_5,-x_6;t). \tag{4.1}$$

This is a consequence of the natural symmetry of the system.

For $b=1.6$ there is one pair of Hopf bifurcation points occurring at mixed-mode equilibrium branches for $x_1^*=12.954$, see figure 2c. Here the imaginary parts $\lambda_i$ of the two complex conjugated eigenvalues with real part zero are $\lambda_i \simeq \pm 0.227$. Consequently, periodic orbits with initial period $T=2\pi/|\lambda_i| \simeq 27.653$ and amplitude zero branch off. The result of the continuation of these periodic orbits as a function of the external forcing is presented in figure 3. It gives the period of the orbits as a function of $x_1^*$.

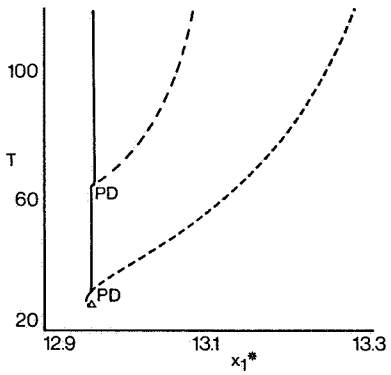


Figure 3. Period $T$ of the periodic orbits as a function of $x_1^*$ for $b=1.6$. Stability properties are denoted by a solid curve (stable) or a dashed curve (unstable). A Hopf bifurcation is indicated by HB, a period-doubling bifurcation by PD.

Clearly, the Hopf bifurcation is subcritical, i.e. a branch of stable equilibria absorbs a branch of unstable periodic orbits. However, already for a slightly smaller external forcing ($x_1^*=12.951$) the periodic orbit merges into a saddle-node bifurcation together with a stable periodic orbit. Next, stable periodic solutions can be found in the range $12.951 \leqslant x_1^* \leqslant 12.9585$. An example of such a solution is shown in figure 4a for $x_1^*=12.958$. This branch of periodic orbits ultimately looses stability in a period-doubling bifurcation at $x_1^*=12.9585$. In figure 4b a stable doubly-periodic solution is shown occurring for $x_1^*=12.9596$. It is found that a sequence of period-doubling bifurcations takes place, leading to the birth of a strange attractor for $x_1^*$ slightly larger than 12.960. A chaotic solution, occurring for $x_1^*=12.961$, is shown in figure 4c.

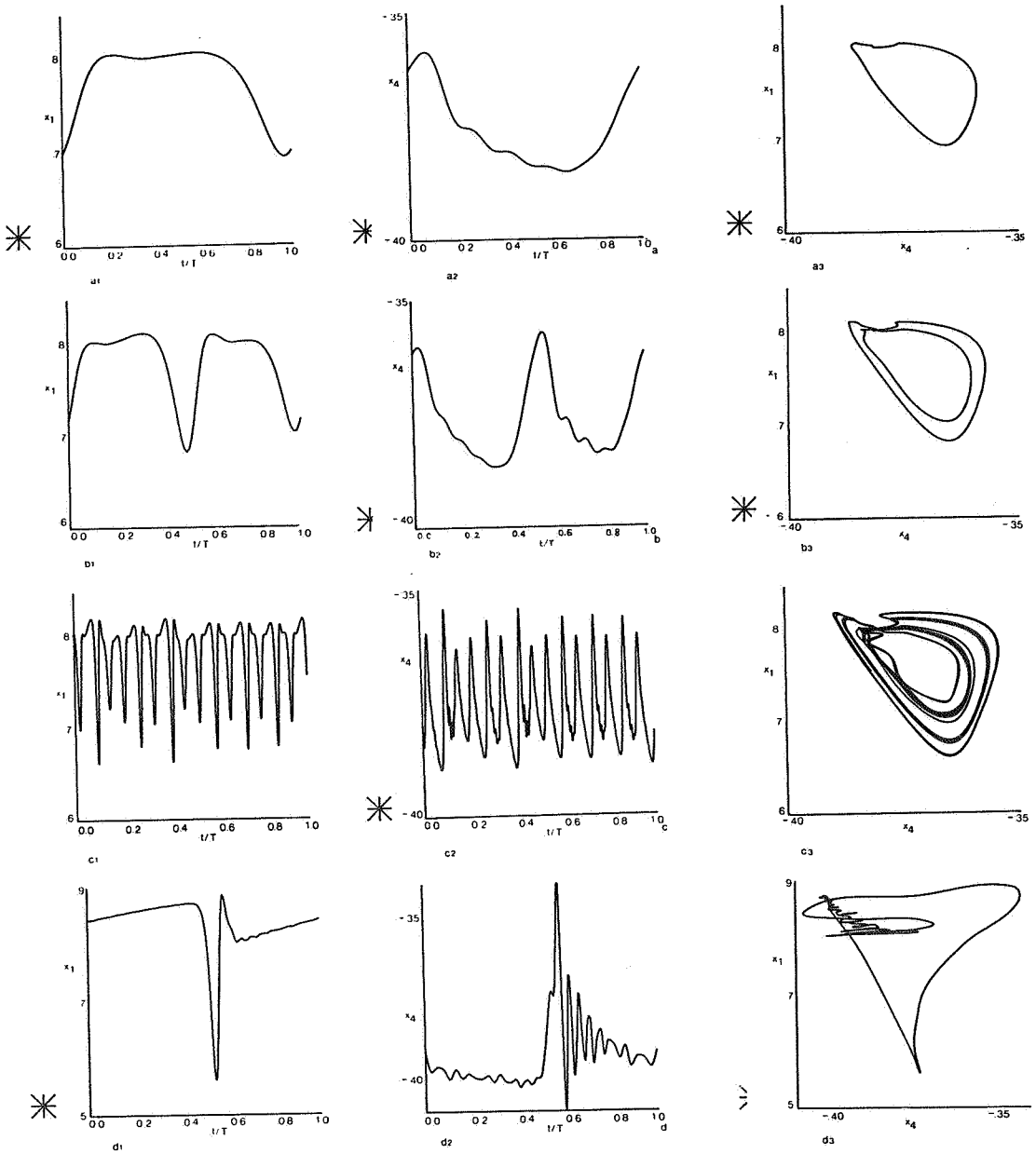

FIGURE 4 a). From left to right: $x_1$ - component of stable periodic solution existing for $b=1.6, x_1^*=12.958$, as a function of $t/T$ (where $T$ is the period), $x_4$-component as a function of $t/T$, and projection of the orbit on to the $x_1-x_4$ plane.

b). As a), but for $x_1^*=12.9596$.

c). Chaotic time series for $b=1.6, x_1^*=12.961$ generated by starting on the unstable principal periodic orbit. From left to right: $x_1$ - component as a function of $t'=(t-1000)/500$, $x_4$-component as a function of $t'$ and projection of the trajectory on to the $x_1-x_4$ plane.

d). Numerical approximation of one of the two homoclinic orbits occurring at $b=1.6, x_1^*=13.26$ as a periodic solution with period $T\to\infty$. From left to right: $x_1$-component as a function of $t/T$, $x_4$-component as a function of $t/T$ and projection of the orbit onto the $x_1-x_4$ plane.

To demonstrate that this signal is truly chaotic we have computed its Lyapunov exponents, following the method of WOLF et al. (1985). They measure the average exponential growth of the principal axes of an infinitesimal small 'error' sphere along the orbit. Chaos is defined by one or more positive Lyapunov exponents which indicate that initially nearby orbits in phase space diverge. The reciprocal of the largest positive exponent defines a time scale on which the system is predictable. In this case it was found numerically that there is one positive Lyapunov exponent $\nu_1 = 0.016$. We have not analysed the strange attractors in detail, since they do not have a global structure. By this we mean that solutions do not show the characteristics of an index cycle. It appears that they remain in the low-index regime permanently.

The region of $x_1^*$ values for which strange attractors occur appears to be very narrow. Numerical integrations show that for $x_1^* \geqslant 12.962$ trajectories starting from arbitrary initial conditions converge to the stable stationary point $E_1$. Obviously the strange attractors have changed into nonattracting strange invariant sets. By this we mean that the chaotic solutions have become unstable and are therefore no longer obtained by means of numerical integrations. Interpreting figure 3, we use some arguments from THOMPSON and STEWART (1986). We hypothesize that the qualitative changes at $x_1^* \simeq 12.962$ are associated with global bifurcations involving heteroclinic connections between the unstable periodic orbits and the saddle points $E_{5a}/E_{5b}$ defined in figure 3c. Next the strange invariant sets disappear in a global bifurcation at $x_1^* \simeq 13.26$. For that parameter value the unstable principal periodic orbits have become homoclinic orbits, which connect the saddle points $E_{5a}$ and $E_{5b}$ with themselves. This bifurcation is called a blue-sky catastrophe because for larger $x_1^*$ values the orbits do no longer exist: they have vanished into the blue sky. A numerical approximation of one of the homoclinic orbits, considered as a periodic orbit with period $T \to \infty$, is shown in figure 4d. The route, which leads to the destruction of a strange attractor for an increasing forcing parameter, is described in SPARROW (1982) as a type-B homoclinic explosion. The reverse route (a type-A homoclinic explosion) *generates* a strange attractor for an increasing forcing parameter. This type of behaviour is for instance found in the famous LORENZ (1963) convection model.

### *4.2. Rossby-mode instabilities*

Next we consider the continuation of periodic orbits generated by Hopf bifurcations for $b = 2$. Then the model behaviour is similar to that studied by CHARNEY and DEVORE (1979). From figure 2d it appears that there is one Hopf bifurcation at a branch of single-mode equilibria ($x_1^* = 1.864$). Furthermore four pairs of Hopf bifurcation points are found at mixed-mode equilibrium branches for $x_1^* = 3.456, x_1^* = 3.229$, $x_1^* = 3.503$ and $x_1^* = 3.623$. The study of periodic solutions generated by these bifurcations will be referred to as case I, case II, case III, case IV and case V, respectively.

In figure 5 the period of the orbits is shown as a function of $x_1^*$ for case I. Part of this bifurcation diagram ($0 < x_1^* < 3.5$) is described in YODEN and HIROTA (1984) and YODEN (1985) and will not be repeated here. For $x_1^* = 3.5$ these authors find chaotic solutions, but no explanation is given on the bifurcation route resulting in the occurrence of a strange attractor. However, using figure 5 we are able to describe the scenario leading to chaos.

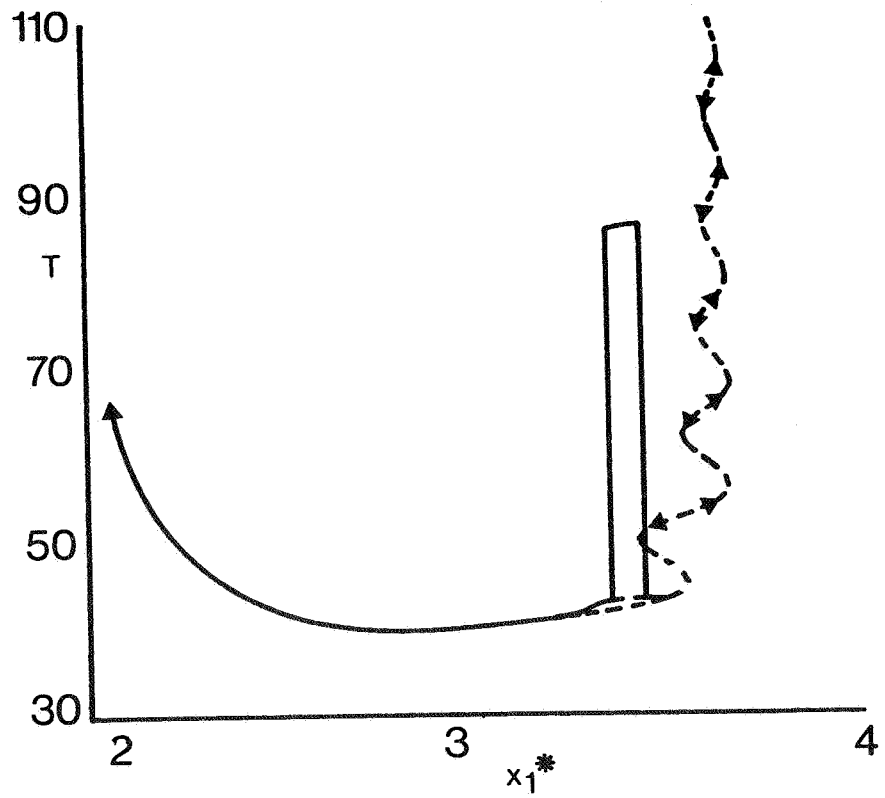


FIGURE 5. Period $T$ of the periodic orbits as a function of $x_1^*$ for $b=2$, case I. Stability properties are indicated by a solid curve (stable) and dashed curve (unstable). Furthermore, BP denotes a pitchfork bifurcation, PD a period-doubling bifurcation and LP a limit point. The symbols $<$ and $>$ indicate a supercritical and subcritical sequence of period-doubling bifurcations in a very small range of $x_1^*$ values.

Briefly the bifurcation structure of the periodic solutions in the region $3.34<x_1^*<3.62$ can be described as follows. Starting from the pitchfork bifurcartion at $x_1^*=3.432$ we arrive for a slightly increased forcing ($x_1^*=3.497$) at a saddle-node bifurcation. Here the branch of stable periodic orbits coalesce with a second branch consisting of unstable periodic orbits which have larger periods. Following the latter branch for decreasing forcing values we encounter a next saddle-node bifurcation at $x_1^*=3.357$ where now a coalescence occurs with a branch of stable periodic orbits. If we continue these stable solutions it appears that they are almost immediately turned unstable by a period-doubling bifurcation. The branch remains unstable until $x_1^*$ is close to a new saddle-node bifurcation existing at $x_1^*=3.615$: for a slightly smaller forcing the branch has become stable due to a period-halving bifurcation. From that moment on the branches of periodic orbits show a similar behaviour as just described, except that the difference between successive saddle-node bifurcation values decrease and that the values of the periods increase. The tendency of the period to become infinitely large is associated with the approach to a homoclinic orbit existing for $x_1^*=3.581$. A numerical approximation of this orbit is shown in figure 6a. It appears that it connects the unstable saddle point $E_3=(0.768,-0.614,-0.234,0.,0.,0.)$ with itself. This type of bifurcation has been analysed by SILNIKOV (1965) and, more recently, by GLENDINNING and SPARROW (1984) and GASPARD et. al. (1984). From their results it follows that in the neighbourhood of the homoclinic orbits a countable infinity of unstable periodic orbits and an uncountable infinity of aperiodic, chaotic orbits exist. The aperiodic

orbits are generated and disappear due to an infinite cascade of period-doubling and periodic-halving bifurcations, respectively. These bifurcations take place near each winding of the $T(x_1^*)$ curve in figure 5. Consequently we possibly have the occurrence of chaotic solutions for parameter values which are close to the critical value at which homoclinity is obtained. Indeed, an example of a chaotic time series, for $x_1^* = 3.5$, is shown in figure 6b. It has one positive Lyapunov exponent $\nu_1 \simeq 0.040$. Note that the trajectories move in a small tube, which closely resembles the homoclinic orbit.

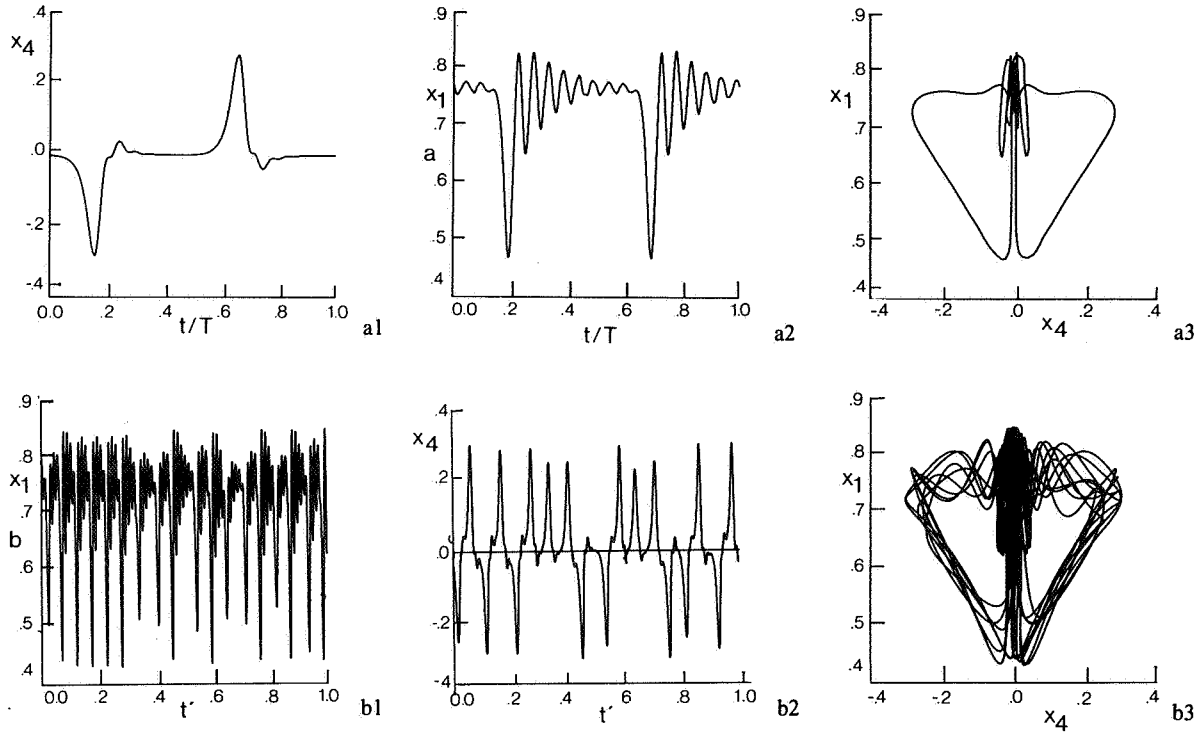


FIGURE 6 a). As figure 4d), but approximation of the homoclinic orbit at $b = 2, x_1^* = 3.581$.
b). As figure 4c), but for $b = 2$ and $x_1^* = 3.5$.

The existence of homoclinic orbits and related chaos is already suggested in figure 1. It was found that codimension-2 bifurcation points occur (A,B,C,D) where a limit point and a Hopf bifurcation point coaslescence. According to LANGFORD (1981) such bifurcations involve homoclinic orbits with an associated direct transition to chaos, see also GUCKENHEIMER and HOLMES (1983) and a remark in LEGRAS and GHIL (1985).

Before discussing the approach to the homoclinic orbit in more detail, we first consider the continuation of periodic orbits which emanate from the pair of Hopf bifurcation points at $x_1^* = 3.456$, (case II). In figure 7 the period of the orbits is plotted as a function of the external forcing. Starting from the subcritical Hopf bifurcations points, with initial period $T \simeq 19.368$, a series of wiggles are found in the interval $3.45 \leqslant x_1^* \leqslant 3.65$. For $x_1^* \simeq 3.584$ we have the approach to two homoclinic orbits. A numerical approximation of one of them is presented in figure 8, the other is obtained by reversing the signs of $x_4, x_5$ and $x_6$, see (4.1). Again they connect the saddle point $E_3$ with itself. In the bifurcation diagram their positions are close to the homoclinic orbit discussed previously. Each of the two new-found orbits seems to be just half a part of the orbit of figure 6a.

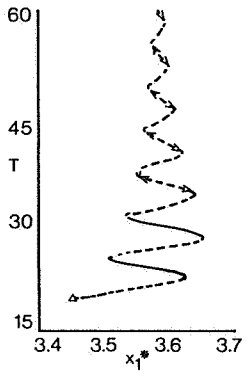


FIGURE 7. As figure 5, but for case II.

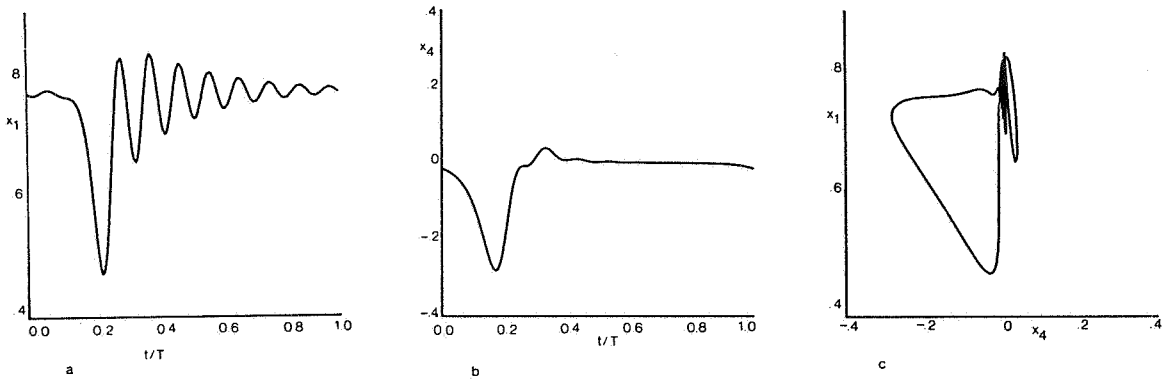


FIGURE 8. As figure 4d), but approximation of one of the homoclinic orbits at $b=2, x_1^*=3.584$.

*4.3. Homoclinic orbits and chaos*

The behaviour of the periodic solutions discussed in the previous subsection can be understood as follows, see GLENDINNING and SPARROW (1984). Suppose that for a parameter value $\mu_{01}$ we have a homoclinic orbit connecting a saddle point with itself, as sketched in figure 9a. The behaviour of the vectorfield close to $\mu_{01}$ is characterized by three eigenvalues of the matrix derivative of the vectorfield, linearized at the saddle point. They are a real positive eigenvalue $\lambda_1$ and two complex conjugated eigenvalues $-\lambda_2 \pm i\omega$ with $\lambda_2 > 0$. If $\lambda_2/\lambda_1 < 1$ the bifurcation diagram of the periodic orbits existing nearby the homoclinic orbit has a similar structure as shown in the figures 5 and 7. However, for nearby parameter values there exist a number of other, so-called subsidiairy homoclinic orbits. They make one or more encounters with the saddle point before returning to it. An example of a double-pulse subsidiary homoclinic orbit is presented in figure 9b. Assume that the saddle-node bifurcations, associated with the approach to an $M$ pulse homoclinic orbit occurring for the parameter value $\mu_{oM}$ are found for parameter values $\{\mu_i\}_{i=1}^{\infty}$ with $\{T_i\}_{i=1}^{\infty}$ the corresponding periods of the orbits. Then

$$\lim_{i\to\infty} (T_{i+1} - T_i) = \frac{M\pi}{\omega}, \tag{4.2a}$$

$$\lim_{i\to\infty} \left[ \frac{\mu_{i+1} - \mu_{oM}}{\mu_i - \mu_{oM}} \right] = -\exp\left[ \frac{-\pi\lambda_2}{\omega} \right], \tag{4.2b}$$

for a derivation see GLENDINNING and SPARROW (1984).

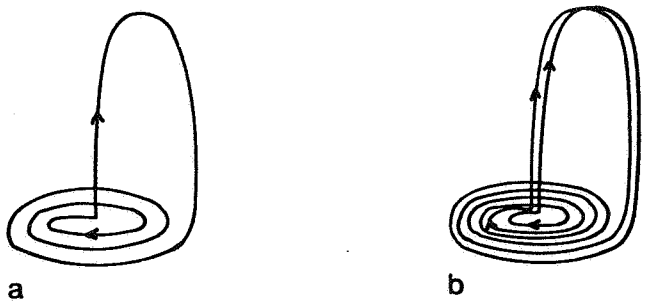


FIGURE 9. Sketches of a principal homoclinic orbit (a) and a double-pulse subsidiairy homoclinic orbit (b).

In our model the numerical values of the three eigenvalues important in this case are

$$\lambda_1 = 0.325\,,\ \lambda_2 = 0.067\,,\ \omega = 1.034. \tag{4.3}$$

We have $\lambda_2/\lambda_1 = 0.206$, which is smaller than 1, as required. Substituting (4.3) in the right-hand sides of (4.2a) - (4.2b) we obtain the numerical values 3.039 M and -0.816, respectively. From the figures 5 and 7 we can find approximations of the left-hand sides of eqa (4.2a) - (4.2b). The results are presented in table 1.

| | figure 5 | figure 7 |
|---|---|---|
| $T_{i+1} - T_i$ | 6.2 | 3.1 |
| $\dfrac{\mu_{i+1} - \mu_{oM}}{\mu_i - \mu_{oM}}$ | -0.89 | -0.81 |

Table 1:
Approximations of the left-hand sides of (4.2a) and (4.2b) from the bifurcation diagrams of figures 5 and 7.

From that we conclude that the two homoclinic orbits occurring at $x_1^* = 3.584$ are principal orbits, while the homoclinic orbit at $x_1^* = 3.581$ is a double-pulse subsidiairy orbit. We remark that $(\mu_{i+1} - \mu_{oM})/\ (\mu_i - \mu_{oM})$ is difficult to compute accurately, because results strongly depend on the parameter value $\mu_{oM}$ for which the homoclinic orbits are found.

*4.4. Bifurcation structure of remaining periodic orbits*

The next case we will study is the continuation of periodic orbits generated due to the Hopf bifurcations at $x_1^* = 3.229$ (case III). In figure 10a the period of these orbits is shown as a function of $x_1^*$. The bifurcation structure is sketched in figure 10b. It can be seen that the branches in this case end in another pair of Hopf bifurcation points occurring at $x_1^* = 3.503$. Consequently, the cases III and IV can be considered together. The bifurcation structure is again rather complicated. Starting from the supercritical Hopf bifurcations at $x_1^* = 3.229$ the branches destabilize at $x_1^* = 3.308$ by means of period-doubling bifurcations. Numerically it is found that this bifurcation is the beginning of an infinite cascade of period-doublings in the region $3.308 \leqslant x_1^* \leqslant 3.3254$, resulting in the generation of a strange attractor. An example of a chaotic time series occurring for $x_1^* = 3.3255$ is shown in figure 11. It has one positive Lyapunov exponent $\nu_1 = 0.012$.

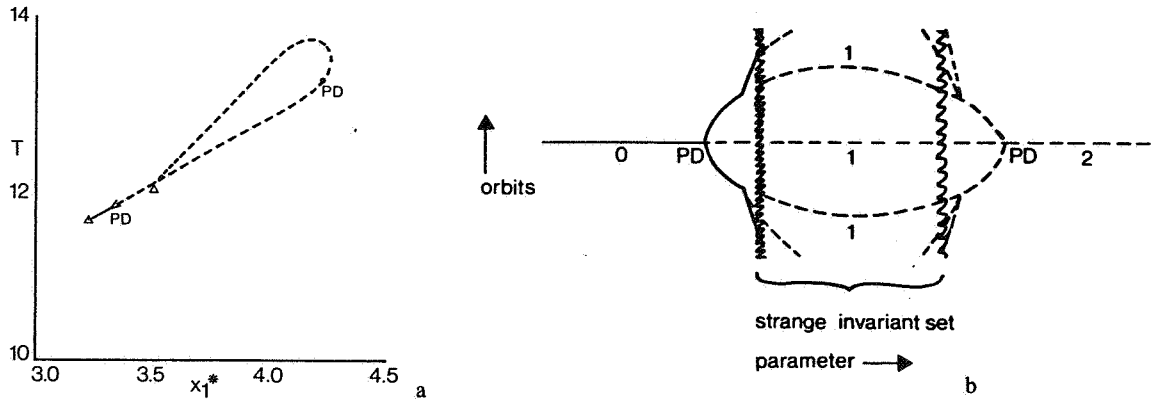


FIGURE 10 a). As figure 5, but for the cases III and IV.
b.) Bifurcation scheme in the region between the period-doubling bifurcations of figure 10a. The straight line denotes the principal periodic orbit. The number of Floquet multipliers (defined in appendix A) with absolute values larger than 1 (which measures the degree of instability of the periodic orbits) is also indicated.

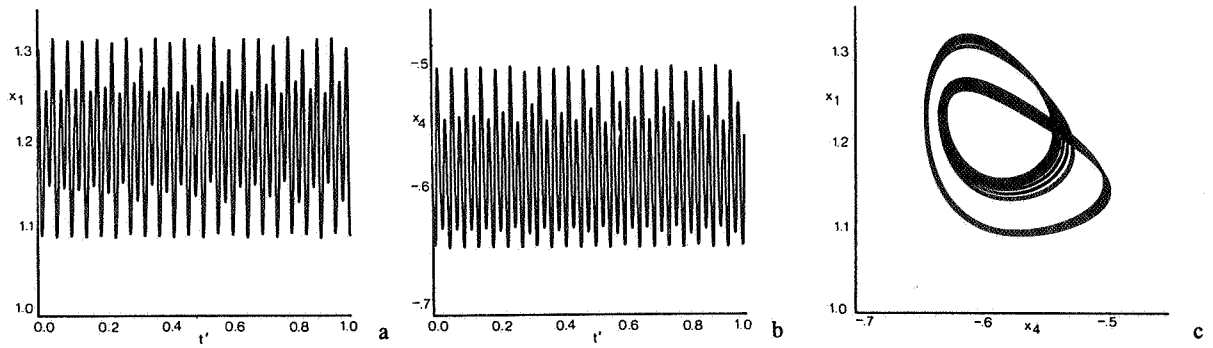


FIGURE 11. As figure 4c), but for $b=2$ and $x_1^*=3.3255$.

It appears that the strange attractors are found in only a narrow range of forcing values. Numerical integrations for $x_1^*$ slightly larger than 3.326 show that trajectories starting close to the unstable principal periodic orbit tend to stable limit cycles with periods close to 86. These limit cycles have already been obtained previously, see figure 5. Obviously at $x_1^* \simeq 3.326$ the strange attractor turns into a nonattracting strange invariant set. Then chaotic solutions still exist, but they are unstable and hence not obtained with numerical integrations. In literature scenarios are known which describe the destabilization of a strange invariant set. They involve heteroclinic connections between unstable stationary points and unstable periodic orbits, see SPARROW (1982) and THOMPSON and STEWART (1986). They are not studied in detail here.

The nonattracting strange invariant sets exist for $3.326 \leqslant x_1^* \leqslant 4.315$, until they disappear in cascades of period-halving bifurcations, the last one occurring at $x_1^* = 4.223$. After that only the principal periodic orbits are left, which have two Floquet multipliers with absolute values larger than 1, see figure 10b. This number indicates the degree of instability of the periodic solution, see appendix A. Next the branches merge into saddle-node bifurcations, together with branches of periodic orbits which originates from the pair of Hopf bifurcation points at $x_1^* = 3.503$.

We finally investigate the periodic orbits, generated by subcritical Hopf bifurcations at $x_1^* = 3.623$ (case V). In figure 12 the period of the orbits is presented as a function of the external forcing parameter. Again a series of wiggles is found, but only in a small region of $x_1^*$ values. This behaviour suggests the approach to homoclinic orbits existing for $x_1^* = 3.625$. A numerical approximation of one of them is shown in figure 13. It seems that these orbits connect the equilibria $E_{6a}/E_{6b} = (1.445, 0.466, -0.182, \mp 0.657, \mp 0.147 \mp 0.024)$ defined in figure 2d with themselves.

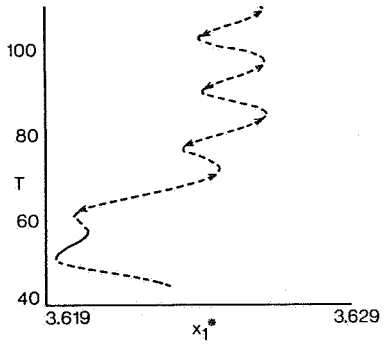


FIGURE 12. As figure 5, but for case V.

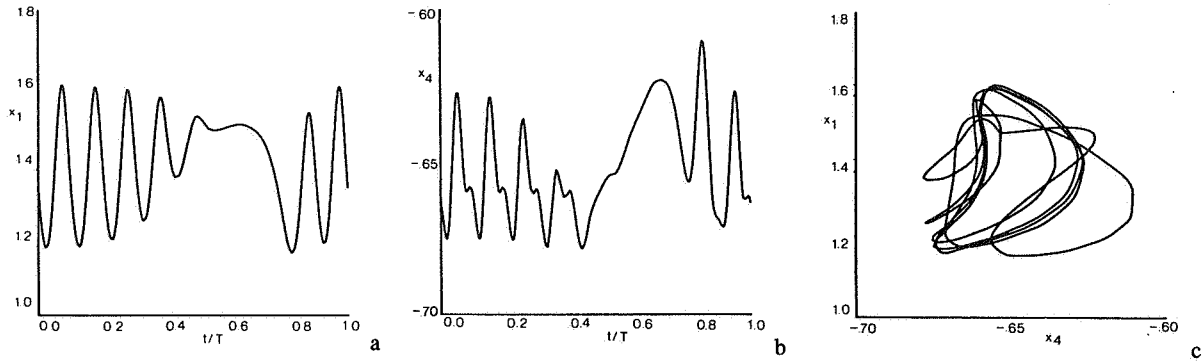


FIGURE 13. As figure 4d, but for $b = 2$ and $x_1^* = 3.625$.

At first sight the bifurcation structure in figure 12 seems to be similar to those of figures 5 and 7. It suggests that the theory discussed in section 4.3 can be applied. However, the normal form of this scenario requires a homoclinic orbit connecting a saddle point in three dimensions. Furthermore, the Jacobian matrix derivative of the vectorfield, linearized at the saddle point, should have one positive real eigenvalue and two complex conjugated eigenvalues with negative real parts. But in this case the saddle points have two real positive eigenvalues as well as two pairs of complex conjugated eigenvalues with negative real parts. Obviously, in order to describe the approach to a homoclinic orbit in figure 12 in a persistent way, the Silnikov theory should probably be generalized to systems of dimensions larger than 3. Another problem comes from the numerically observed fact that in most cases trajectories starting close to the unstable principal periodic orbits appear not to be chaotic. Instead they tend to one of the stable equilibria $E_{4a}$ or $E_{4b}$. Thus the scenario leading to the bifurcation structure shown in figure 12 remains to be investigated.

## 5. THE POSSIBILITY OF INDEX CYCLES

In order for the spectral system (2.11) to model the large-scale atmospheric circulation it should have at least qualitative agreement with synoptic observations. Therefore, we expect the system to fluctuate irregularly between different preference domains in phase space. So for we have found irregular chaotic solutions for certain parameter values and initial conditions, but they remain in the low-index circulation regime forever. The corresponding strange attractors in phase space appear to have a small

size and, moreover, have small attraction domains. Consequently, there is only a small set of initial conditions for which trajectories are attracted to a strange invariant set. For the concept of deterministic chaos to be physically meaningful the strange attractor should have a global structure in phase space. In other words, chaotic trajectories should be capable of visiting both the low-index and high-index regimes. Such a system would show the characteristics of an index cycle. A recent discussion about this phenomenon can be found in HOSKINS and PEARCE (1983). In our model an index cycle is not found, because the high-index equilibrium $E_1$ is stable for all parameter values. This is due to the fact that the equilibrium is dominated by a (0,1) zonal flow component. It cannot be destabilized by topographic instability since this mechanism only acts on wave modes. Furthermore, barotropic instability of the (0,1) mode is forbidden by the Fjørtoft theorem (FJØRTOFT, 1953) because it has the smallest wave-number of the spectrum.

However, with a slight extension of the model it is possible to obtain unstable high-index equilibria. This is done by adding a forcing term $Cx_4^*$ to the right hand side of the equation for $\dot{x}_4$ in (2.11). In this way the (0,2) zonal flow component of $E_1$ is externally forced. For sufficiently large $x_4^*$ and $b<\sqrt{3}$ this mode can become barotropically unstable, see (2.13) and appendix B. As an example we take the numerical values $b=1.6, C=0.1, \beta=1.25$, $\gamma=1, x_1^*=4$ and let $x_4^*$ be a free parameter. In appendix B a lower bound is computed of the critical amplitude $|x_{4,c}^*|$ for which barotropic instability of the high-index equilibrium will occur. It is found that $|x_{4,c}^*|$ should be somewhat larger than 0.35. In figure 14 the results of a numerical bifurcation analysis are presented. They show the $\hat{x}_4$ components of the equilibria as a function of $x_4^*$, where for $x_4^*=0$ is started in the equilibria $E_1, E_2$ and $E_3$, respectively.

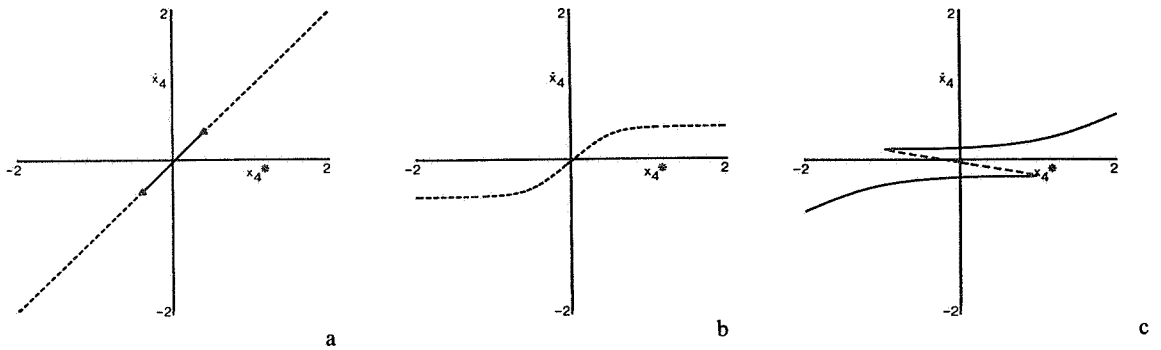


FIGURE 14. $\hat{x}_4$-component of the equilibria for $b=1.6$ and $x_1^*=4$ as a function of $x_4^*$. For $x_4^*=0$ a restart is made in $E_1(a), E_2(b)$ and $E_3(c)$. Stability properties are indicated by a solid line (stable) or dashed line (unstable). The triangle symbol denotes a Hopf bifurcation point.

Considering $E_1$, it becomes barotropically unstable at $|x_{4,c}^*|=0.402$ by means of a Hopf bifurcation. Next we have investigated the continuation of periodic orbits emanating from the equilibrium branches. Starting from the bifurcation points stable periodic orbits are found with increasing $|x_4^*|$. At $|x_4^*|=8.459$ they loose stability because of a period-doubling bifurcation. However, at $|x_4^*|=11.771$ they become stable again by absorbing a branch of unstable doubly-periodic orbits. The principal periodic orbits ultimately loose stability at $|x_4^*|=19.705$ by means of a bifurcation to a torus. The branches of doubly-periodic orbits have a complicated structure and appear to be unstable for almost all parameter values.

We have investigated the existence of strange attractors in the range $0<|x_4^*|<15$. It was found that trajectories either tend to a limit cycle of the high-index type or to a stationary point of the low-index type, but no chaotic solutions were obtained. The existence of point attractors can be understood

from figure 14b,c. It appears that the equilibrium $E_2$ remains unstable if $x_4^*$ is varied, but always a stable equilibrium of the low-index type is found. When $|x_4^*|$ is large most energy of these equilibria is contained in the (1,1) wave mode. This mode cannot become unstable because the model contains only one wave triad, for which (2.13) holds, and here $b < \sqrt{3}$. Thus, the conclusion is that the six-component barotropic spectral model (2.11) cannot generate index cycles.

## 6. Summary and conclusions

We have studied a six-component spectral model of the barotropic potential vorticity equation in a beta plane channel, originally introduced by Charney and DeVore (1979). In order to investigate in what sense the model reflects features of the atmospheric circulation, a systematic bifurcation analysis has been carried out for two free parameters. They are the external forcing and the width-length ratio of the channel which control the topographic and barotropic instability mechanisms, respectively. It is concluded that the physical and mathematical properties of the model are richer than those of the three-component subsystem. In both models multiple equilibria can occur for fixed parameter values. The associated streamfunction patterns resemble large-scale preference states of the atmospheric circulation. However, the nontransient solution behaviour in the subsystem is always stationary, whereas for the full model also periodic, quasi-periodic and chaotic solutions are found. In particular the occurrence of strange attractors is of interest since the associated solutions model an irregular time-dependent flow. Furthermore, chaos is characterized by sensitive dependence on the initial conditions: nearby orbits in phase space exponentially diverge during the evolution of the system. Since in practical situations initial conditions are never known with infinite precision, the system evolution can only be predicted for a finite amount of time. A finite predictability is typically one of the properties of the atmospheric circulation. This follows from numerical experiments as well as from theoretical studies (Holloway and West, 1984).

Various scenarios are found which describe the generation or destruction of a strange attractor. Apart from the period-doubling route we obtained homoclinic orbits in a few cases, which connect unstable stationary points with themselves. For nearby parameter values chaotic orbits trajectories occur moving in small tubes around the homoclinic orbits. This is in agreement with Silnikov's theory, see Sparrow (1982) and Glendinning and Sparrow (1984).

Despite its complexity and interesting properties the validity of the model is limited. It appears that the strange attractors do not have a global structure in the sense that chaotic trajectories are capable of visiting alternately different preference regions in phase space. Thus, it is concluded that the model (2.11) cannot show vacillatory behaviour. The reason is clearly due to a lack of barotropic wave triads or, equivalently, due to the severe truncation. Internal vacillation can only be obtained by allowing quasi-statically changes of the parameters. This can be considered as modelling slowly varying boundary conditions of the model, see Legras and Ghil (1985).

For fixed parameter values vacillation can be generated in three ways. The first is to add stochastic perturbations to the eqa. (2.11), see de Swart and Grasman (1987). The second way consists of constructing a spectral model with more degrees of freedom by allowing more eigenfunctions in the spectral expansions, as was done by Legras and Ghil (1985). The third possibility is to consider spectral models of baroclinic flows, see Charney and Straus (1980) and Reinhold and Pierrehumbert (1982).

## References

[1] Charney J.G. and J.G. DeVore, 1979, *Multiple flow equilibria in the atmosphere and blocking.* J. Atmos. Sci. 36, 1205-1216.

[2] Charney J.G. and D.M. Straus, 1980: *Form-drag instability, multiple equilibria and propagating planetary waves in baroclinic, orographically forced, planetary wave systems,* J. Atmos. Sci. 37, 1157-1176.

[3] De Swart H.E., 1987 *Low-order spectral models of the atmospheric circulation.* Acta Appl. Math,

in press.

[4] DE SWART H.E. and J. GRASMAN, 1987: *Effect of stochastic perturbations on a low-order spectral model of the atmospheric circulation.* Tellus **39A**, 10-24.

[5] DOEDEL E., 1986: *AUTO 86 user manual, software for continuation and bifurcation problems in ordinary differential equations.* Concordia University, Montreal.

[6] FJØRTOFT R. 1953: *On the changes in the spectral distribution of kinetic energy for two-dimensional, nondivergent flow.* Tellus **5**, 225-230.

[7] GASPARD P., R. KAPRAL and G. NICOLIS, 1984: *Bifurcation phenomena near homoclinic systems: a two-parameter analysis.* J. Stat. Phys. **35**, 697-727.

[8] GLENDINNING P. and C. SPARROW, 1984: *Local and global behaviour near homoclinic orbits.* J. Stat. Phys. **35**, 645-697.

[9] GUCKENHEIMER J. and P. HOLMES, 1983: *Nonlinear oscillations, dynamical systems, and bifurcations of vector fields.* Springer Verlag, 453 pp.

[10] HAARSMA R.J. and J.D. OPSTEEGH, 1987: *Instability mechanisms of the shallow-water equations.* Subm. to J. Atmos. Sci..

[11] HOLLOWAY G. and B.J. WEST (eds.), 1984: *Predictability of fluid motions.* Am. Inst. Phys., 612 pp.

[12] HOSKINS B.J. and A.P. PEARCE (eds.), 1983: *Large scale dynamical processes in the atmosphere.* Academic Press, 397 pp.

[13] KÄLLÉN E. 1981: *The nonlinear effects of orographic and momentum forcing in a low-order, barotropic model.* J. Atmos. Sci. **38**, 2150-2163.

[14] KÄLLÉN E. 1982: *Bifurcation properties of quasi-geostrophic, barotropic models and their relation to atmospheric blocking.* Tellus **34**, 255-265.

[15] LANGFORD W.F. 1981: *A review of interactions of Hopf and steady-state bifurcations.* In: Barenblatt, G.I., G. Ioos and D.D. Joseph (eds.), Nonlinear dynamics and turbulence, Pitman, 215-237.

[16] LEGRAS B. and M. GHIL, 1985: *Persistent anomalies, blocking and variations in atmospheric predictability.* J. Atmos. Sci. **42**, 433-471.

[17] LORENZ E.N. 1963: *Deterministic nonperiodic flow.* J. Atmos. Sci. **20**, 130-141.

[18] LORENZ E.N. 1969: *The predictability of a flow which possesses many scales of motion.* Tellus **21**, 289-307.

[19] MATSUDA Y. 1983: *Classification of critical points and symmetry-breaking in fluid phenomena and its application to dynamic meteorology.* J. Meteor. Soc. Japan **61**, 771-788.

[20] PEDLOSKY J. 1979: *Geophysical fluid dynamics.* Springer Verlag, 624 pp.

[21] PHILLIPS N.A. 1954: *Energy transformations and meridional circulations associated with simple baroclinic waves in a two-level, quasi-geostrophic model.* Tellus **6**, 273-286.

[22] REINHOLD B.B. and R.T. PIERREHUMBERT, 1982: *Dynamics of weather regimes: quasi-stationary waves and blocking.* Mon. Wea. Rev. **110**, 1105-1145.

[23] SILBERMAN I. 1954: *Planetary waves in the atmosphere.* J. Meteor. **11**, 27-34.

[24] SILNIKOV L.P. 1965: *A case of the existence of a denumerable set of periodic motions.* Sov. Math. Dokl. **6**, 163-166.

[25] SPARROW C. 1982: *The Lorenz equations: bifurcations, chaos and strange attractors.* Springer Verlag, 269 pp.

[26] THOMPSON J.M.T. and H.B. STEWART, 1986: *Nonlinear dynamics and chaos,* John Wiley & Sons, 376 pp.

[27] WOLF A., J.B. SWIFT, H.L. SWINNEY and J.A. VASTANO, 1985: *Determining Lyapunov exponents from a time series.* Physica **16D**, 285-317.

[28] YODEN S. and I. HIROTA, 1984: *A numerical study on periodic and chaotic behaviour in a geophysical fluid system.* In: T. Tatsumi (ed.), Turbulence and chaotic phenomena in fluids, Elsevier Science, 477-482.

[29] YODEN S. 1985: *Bifurcation properties of a quasi-geostrophic, barotrophic, low-order model with topography.* J. Meteor. Soc. Japan **63**, 535-546.

# Appendix A: Bifurcation analysis of spectral models

Consider a spectral model which is a dynamical system of the type (1.1). We will briefly discuss that the existence of strange attractors can be investigated from a systematic bifurcation analysis of its stationary points and periodic orbits. For more details we refer to GUCKENHEIMER and HOLMES (1983) and THOMPSON and STEWART (1986). The smooth vectorfield $f_\mu(x)$ generates a phase flow $\phi^t:\mathbb{R}^N\to\mathbb{R}^N$. Then $x(t)=\phi^t x_0$ defines an orbit or a trajectory of (1.1) in phase space having the initial condition $x(0)=x_0$. It is well-known that these solutions exist and are unique. The spectral model in this paper obeys

$$\nabla\cdot f_\mu(x) = -a \;\; ; \;\; a>0, \tag{A1}$$

indicating that small volume elements in phase space always shrink. Moreover it can be shown that its solutions are bounded.

Stationary points $\hat{x}$ satisfy

$$f_\mu(\hat{x}) = 0 \tag{A2}$$

and the system is said to be in equilibrium or in a steady state. The dynamics of small perturbations $x'$ on this state is described by

$$\dot{x}' = \underline{\underline{D}}\cdot x' + o(|x'|), \;\; (\underline{\underline{D}})_{ij} = \partial f_{\mu,i}/\partial x_j \,|_{x=\hat{x}} . \tag{A3}$$

As long as the eigenvalues $\{\lambda_i\}_{i=1}^N$ of matrix $D$ have no zero real parts they govern the stability of $\hat{x}$. If all real parts are negative $\hat{x}$ is stable, whereas if at least one eigenvalue has a positive real part the stationary point is unstable. Since the system obeys (A1) the sum of all eigenvalues equals $-a$, which is negative. Consequently unstable equilibria are of the saddle-point type: they have a stable manifold $W^s(\hat{x})$ as well as an unstable manifold $W^u(\hat{x})$, defined as

$$\begin{aligned} W^s(\hat{x}) &= \{x\in\mathbb{R}^N \,|\, \phi^t x\to\hat{x} \text{ for } t\to\infty\}, \\ W^u(\hat{x}) &= \{x\in\mathbb{R}^N \,|\, \phi^t x\to\hat{x} \text{ for } t\to-\infty\}. \end{aligned} \tag{A4}$$

Near the stationary point $W^s(\hat{x})(W^u(\hat{x}))$ is spanned by the eigenvectors corresponding to the eigenvalues of matrix $D$ with negative (positive) real part. It may occur that a stable manifold of a stationary point $\hat{x}^{(i)}$ is contained in an unstable manifold of a stationary point $\hat{x}^{(j)}$ or vice versa. If $i=j(i\neq j)$ this gives rise to homoclinic (heteroclinic) connections, see figure A1.

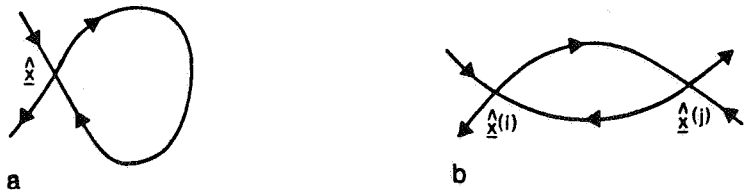


FIGURE A1: Visualization of homoclinic (a) and heteroclinic connections (b).

A procedure to compute branches of stationary points as a function of one control parameter $\mu_1$ numerically is described in LEGRAS and GHIL (1985). The method is implemented in the package AUTO of DOEDEL (1986) which is used in this paper. Generally, in this way we will encounter critical parameter values where one or more real parts of the eigenvalues of matrix $D$ become zero. Near these bifurcation points we can no longer neglect the $o(|x'|)$ contributions in (A3). Important information about the behaviour of the dynamical system near such a point is provided by two theorems. The first states that the local behaviour is governed by the projection of the system onto the center manifold, which is locally spanned by the eigenvectors corresponding to the eigenvalues of $D$ with zero real part. The second theorem states that the projected system can be transformed into a limited number of standard (normal) forms. In case of one control parameter $\mu_1$ (codimension 1 bifurcations) there are four normal forms for the local bifurcations of stationary points. They read

$$\dot{x}_1 = \mu_1 + \alpha x_1^2 \quad : \quad \text{saddle-node bifurcation,} \tag{A5a}$$

$$\dot{x}_1 = \mu_1 x + \alpha x_1^2 \quad : \quad \text{transcritical bifurcation,} \tag{A5b}$$

$$\dot{x}_1 = \mu_1 x + \alpha x_1^3 \quad : \quad \text{pitchfork bifurcation,} \tag{A5c}$$

$$\left.\begin{aligned} \dot{r} &= \mu r + a r^3 \quad , r^2 = x_1^2 + x_2^2 \\ \dot{\theta} &= 1 \qquad\quad , \tan\theta = x_2/x_1 \end{aligned}\right] \quad : \quad \text{Hopf bifurcation.} \tag{A5d}$$

Here $\alpha$ can have the values $-1$ or 1, which refer to a supercritical and subcritical bifurcation, respectively. The behaviour of the solutions of (A5) for $\alpha = -1$ is shown in figure A2.

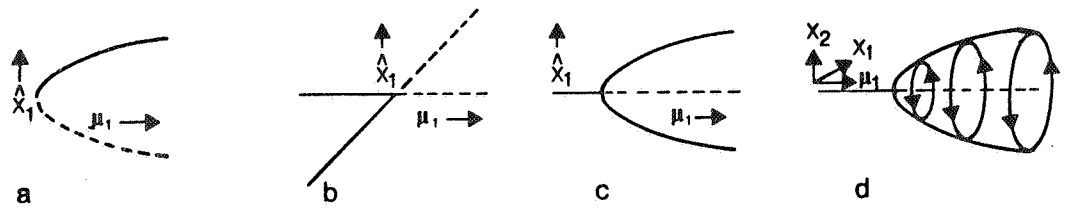


FIGURE A2. Bifurcation diagram of the supercritical saddle-node bifurcation (a), transcritical bifurcation (b), pitchfork bifurcation (c) and Hopf bifurcation (d). A solid line denotes that the solution is stable whereas a dashed line refers to an unstable solution.

The first three types correspond to a real eigenvalue passing through zero at $\mu_1 = 0$. In case of the saddle-node bifurcation $(\hat{x}_1, \mu_1) = (0,0)$ is not a singular point of the vectorfield since its derivative with respect to $\mu_1$ is nonzero. Therefore it is called a limit point whereas in all other cases $(\hat{\underline{x}}, \mu_1) = (0,0)$ is a

bifurcation point. The pitchfork bifurcation requires invariance under the transformation $x_1 \to -x_1$. Finally the Hopf bifurcation generates a periodic orbit which at $\mu_1 = 0$ has amplitude zero and period $T = 2\pi/\lambda^{(i)}$, where $\pm\lambda^{(i)}$ are the imaginary parts of the eigenvalues of $D$ with real parts zero.

However, more complicated situations may occur, where one than one control parameter is needed to describe the bifurcation adequately. A frequently occurring example is the case of a saddle-node bifurcation where the quadratic terms become nonzero ($\alpha = 0$ in (A5a)). Then the generalized normal form

$$\dot{x}_1 = \mu_1 + \mu_2 x_1 + \alpha x_1^3 \tag{A6}$$

should be considered. This unfolding of the saddle-node bifurcation describes a codimension-2 bifurcation since we now have two control parameters instead of one. The set of bifurcation values $(\mu_1, \mu_2)$ consists of two branches describing saddle-node bifurcations which coalesce at the cusp point $(\mu_1, \mu_2) = (0,0)$. Other complicated situations occur when matrix $D$ in (A3) is more degenerated, for example that one real eigenvalue as well as the real parts of the complex conjugated eigenvalues become zero for a specific parameter value. As shown by LANGFORD (1981) the bifurcation structure may then involve homoclinic and heteroclinic connections, which are associated with a direct transition from regular to chaotic solutions.

We next consider the stability of $T$-periodic orbits $\gamma(t)$ of (1.1), thus $\gamma(t+T) = \gamma(t)$. The dynamics of small perturbations on this orbit is given by

$$\dot{x} = \underline{\underline{A}}(t) \cdot x' + o(|x'|), \quad [\underline{\underline{A}}(t)]_{ij} = \partial f_{\mu,i} / \partial x_j |_{\gamma(t)} \tag{A7}$$

Since $A(t)$ is a periodic matrix the linear part of (A7) is solved by defining as fundamental matrix $\Phi(t)$ with elements

$$[\underline{\underline{\Phi}}(t)]_{ij} = \partial x_i / \partial x_j |_{\gamma(t)} \tag{A8}$$

The columns of this matrix contain $N$ independent solutions of the linearized system in (A7). The eigenvalues $\{\rho_i\}_{i=1}^N$ of matrix $\Phi(T)$ are called Floquet multipliers. One of them (say $\rho_1$) is always equal to one. As long as all other multipliers have absolute values not equal to one they govern the stability of $\gamma(t)$. If all absolute values are smaller than 1 the periodic orbit is stable, whereas if at least one of the multipliers has absolute value larger than one $\gamma(t)$ is unstable. A numerical procedure to compute periodic orbits as a function of a control parameter is discussed in SPARROW (1982). Besides we have used the continuation routines of AUTO of DOEDEL (1986).

Bifurcations of periodic orbits can be analysed in a similar way as discussed for stationary points. In case of one control parameter there now appear to be five normal forms. Three of them correspond to a real Floquet multiplier passing through 1 and are again called a saddle-node, transcritical and pitchfork bifurcation. Their bifurcation diagrams are similar to those of figure $A2^{a-c}$ except that $\hat{x}_1$ should be replaced by the period $T$ of the orbit. If a real Floquet multiplier passes through $-1$ a period-doubling bifurcation occurs. In the supercritical case, see figure A $3^a$, we have for $\mu_1 < 0$ a stable $T$-periodic orbit. It becomes unstable at $\mu_1 = 0$, thereby generating a stable $2T$-periodic orbit. The final possibility is that the absolute values of two complex conjugated multipliers become 1 at $\mu_1 = 0$. This situation corresponds to a transition from stable periodic to stable quasi-periodic motion, where the latter is characterized by two fundamental frequencies having an irrational ratio.

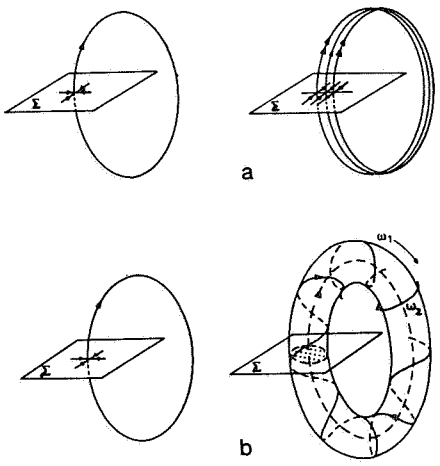


FIGURE A3. Phase-flow behaviour for $\mu_1 < 0$ (left) and $\mu_1 > 0$ (right) in case of the supercritical period-doubling bifurcation (a) and torus bifurcation (b). Here $\Sigma$ is a plane chosen such that it is intersected by the orbits.

There are several bifurcation scenarios which lead to the generation of strange attractors with associated chaotic motion. A frequently occurring example is the period-doubling route, where in a finite interval of the control parameter domain an infinitely long sequence of period-doubling bifurcations occurs, which beyond the accumulation point $\mu_1^c$ result in chaotic motion. Another way to obtain chaos is that a periodic orbit becomes homoclinic such that it connects a saddle point with itself. SILNIKOV (1965) first showed that for parameter values close to the homoclinic point chaotic orbits exist. This scenario is discussed in more detail in section 4 of this paper. Anyway, it appears that considering bifurcation properties of stationary points and periodic orbits is a way to investigate the existence of strange attractors.

# Appendix B: Stability of zonal-flow profiles

In HAARSMA and OPSTEEGH (1987) a method is developed to study the stability of zonal-flow profiles. In this appendix the theory is extended to forced and dissipative systems, as well as to more complicated flow profiles. It can then be applied to the barotropic spectral model (2.11).

Consider the barotropic potential vorticity equation (2.1) for $\gamma=0$ and $\psi^*=\psi^*(y)$. Then $\hat{\psi}=\psi^*$ is a stationary solution of the equation.

The stability of the solution is investigated by considering the dynamics of small perturbations $\psi'$ on $\hat{\psi}$. We obtain

$$(\frac{\partial}{\partial t}+u^*\frac{\partial}{\partial x})\nabla^2\psi' + (\beta-\frac{d^2u^*}{dy^2})\frac{\partial\psi'}{\partial x} + C\nabla^2\psi' = 0, \quad u^*(y) = -\frac{d\psi^*}{dy}. \tag{B2}$$

In the $\beta$-channel geometry with the boundary conditions (2.8) each solution of the barotropic potential vorticity equation can be expanded in eigenfunctions defined in (2.10). In this case, because of (B1) and (B2), we have

$$u^* = \sqrt{2}\sum_{l=1}^{\infty} u_l^* \sin(\frac{ly}{b}) \; ; \; u_l^* = \frac{l\psi_l}{b}, \tag{B3a}$$

$$\psi' = \{\sqrt{2}\sum_{l=1}^{\infty}\psi_l'\cos(\frac{ly}{b}) + \sum_{n=1}^{\infty}\sum_{m=1}^{\infty}\psi_{nm}'\, e^{inx}\sin(\frac{my}{b})\}e^{-i\sigma t}, \tag{B3b}$$

where $u_l^*$ and $\psi_l'$ are real coefficients, while $\psi_{nm}'$ will be complex amplitudes. We ask for conditions resulting in growing perturbations. i.e.

$$\mathrm{Im}(\sigma)>0. \tag{A4}$$

Substituting (B3a) and (B3b) in (B2) and projecting on the spectral components we obtain

$$\{\psi_l' = 0\}_{l=1}^{\infty}, \tag{B5a}$$

$$\{(\sigma+iC)(n^2+\frac{m^2}{b^2})+n\beta\}\psi_{nm}' + \sum_{q=1}^{\infty}\sum_{l=1}^{\infty} nu_l^*(n^2+\frac{q^2-l^2}{b^2})c_{mlq}\,\psi_{nq}' = 0 \begin{matrix} n=1,2,\cdots, \\ m=1,2,\cdots, \end{matrix} \tag{B5b}$$

with

$$c_{mlq} = \begin{cases} \frac{\sqrt{2}}{\pi}\{\frac{1}{m+l+q} + \frac{1}{m-l-q} - \frac{1}{m+l-q} - \frac{1}{m-l+q}\} & , m+l+q \text{ odd}, \\ 0 & , m+l+q \text{ even}. \end{cases} \tag{B6}$$

We now apply this method to the truncated barotropic spectral model (2.11). Here $m,l$ and $q$ can take on the values 1 and 2, while $n=1$. The eqa. (B5b) reduce to

$$[(\sigma+iC)\kappa_1^2+\beta-\alpha_1 u_1^*]\psi_{11}' - \tfrac{1}{2}\tilde{u}_2\,\psi_{12}' = 0, \tag{B7a}$$

$$-\tfrac{1}{2}\tilde{u}_2(1-\kappa_2^2+\kappa_1^2)\psi_{11}' + [(\sigma+iC)\kappa_2^2+\beta-\alpha_2 u_1^*]\psi_{12}' = 0, \tag{B7b}$$

where

$$\begin{aligned}&\kappa_1^2 = 1+\frac{1}{b^2}\quad,\ \kappa_2^2 = 1+\frac{4}{b^2},\\ &\alpha_1 = \frac{32\sqrt{2}}{15\pi}(1+\frac{3}{b^2})\ ,\ \alpha_2 = \frac{8\sqrt{2}}{3\pi},\tilde{u}_2 = 64\frac{\sqrt{2}}{15\pi}\,u_2^*.\end{aligned} \tag{B8}$$

For nontrivial solutions of (B7a-B7b) the determinant of the coefficient matrix must be zero. This results in the quadratic equation

$$a_2\mu^2 + a_1\mu + a_0 = 0 \tag{B9}$$

where

$$\begin{aligned}&\mu = \sigma + iC \quad ,\quad a_2 = \kappa_1^2\kappa_2^2,\ a_1 = (\beta-\alpha_1 u_1^*)\kappa_1^2 + (\beta-\alpha_2 u_1^*)\kappa_2^2,\\ &a_0 = (\beta-\alpha_1 u_1^*)(\beta-\alpha_2 u_1^*) - \tfrac{1}{4}\,\tilde{u}_2^2(1-\kappa_2^2+\kappa_1^2).\end{aligned} \tag{B10}$$

From (B4) and the solutions of(B9) it then follows that the zonal-flow profile is unstable if

$$a_1^2 - 4a_0a_2 \leqslant -(2a_2C)^2\,. \tag{B11}$$

Solving for $\tilde{u}_2$ gives

$$\tilde{u}_2^2 > \frac{(2\kappa_1^2\kappa_2^2C)^2 + \{\beta(\kappa_2^2-\kappa_1^2)-(\alpha_2\kappa_2^2-\alpha_1\kappa_1^2)u_1^*\}^2}{(\kappa_2^2-\kappa_1^2-1)\kappa_1^2\kappa_2^2} = (u_{2,c}^*)^2 \tag{B12}$$

As a numerical example we have taken $b=1.6, C=0.1, \beta=1.25$, $u_1^*=x_1^*=4$ and we ask for the critical amplitude

$$x_{4,c}^* = \tfrac{1}{2}u_2^* = \frac{15\pi}{128\sqrt{2}}\tilde{u}_2, \tag{B13}$$

see (2.12), (B3a) and (B8). Substituting the values in (B12) and developing (B13) we obtain

$$|x_4^*| > x_{4,c}^* = 0.3471. \tag{B14}$$

This agrees with the results of a numerical bifurcation analysis of the spectral model for the same parameter values.

For nonzero $\gamma$ we still expect the theory presented here to have some validity for the high-index equilibrium. Although the flow is no longer purely zonal, the wave amplitudes are small compared to the zonal-flow components. Because the waves have extracted energy the effective $u_1^*$ in (B12) will be smaller. Since

$$\alpha_2\kappa_2^2 - \alpha_1\kappa_1^2 = \frac{8\sqrt{2}}{15\pi}\,\frac{(b^2-2)(b^2+6)}{b^4}$$

is positive for $b=1.6$ we expect the effective (0,2) velocity component to be somewhat larger than in case $\gamma=0$. This is confirmed by numerical experiments, which show for $\gamma=1$ a (0,2) amplitude $|\hat{x}_4|=0.393$ with a corresponding critical forcing $|x_{4,c}^*|=0.402$.